Gradient doping of Cu(I) and Cu(II) in ZnO nanorod photoanode by electrochemical deposition for enhanced photocurrent generation

F.Z. Nouasria, D. Selloum, A. Henni, D. Zerrouki, Sophie Tingry

Gradient doping of Cu(I) and Cu(II) in ZnO nanorod photoanode by electrochemical deposition for enhanced photocurrent generation

F. Z. Nouasria[1], D. Selloum [1], A. Henni [1*], D. Zerrouki [1], S. Tingry [2]

[1] *Lab. Dynamic Interactions and Reactivity of Systems, Kasdi Merbah University, Ouargla 30000, Algeria.*

[2] *Institut Européen des Membranes, UMR 5635, Université Montpellier, ENSCM, CNRS, Montpellier, France*

*** Corresponding author.** Abdellah Henni

E-mail address: henni.abdellah@gmail.com, henni.abdellah@univ-ouargla.dz

Abstract

This study describes the synthesis and characterization of Cu-doped ZnO nanorods (NRs) by an electrochemical method in the presence of two different Cu precursor (Cu^{+2} and Cu^{+}) in order to improve photocurrent generation. Analyses of the resulting materials by X-ray diffraction (XRD), scanning electron microscopy (SEM), UV-Vis and electrochemical photocurrent (ECP) spectroscopy confirm the formation of well-aligned ZnO Würtzite nanostructures in the form of hexagonal rods. For both doping source with a concentration of up to 0.5%, the following changes were observed: a distortion of the ZnO morphology, an increase in transmittance to 96% for ZnO doped with Cu^{+2}, and a reduction of the energy gap from 3.36 eV to 3.06 and 3.02 eV for ZnO doped with Cu^{+2} and Cu^{+}, respectively. From photoelectrochemical tests, the photo-current density was improved up to 0.05 $mA.cm^{-2}$ in the presence of Cu doping, which is twelve times superior to that of undoped ZnO nanorods, which means that the incorporation of Cu^{+2} or Cu^{+} significantly improves the separation efficiency of photogenerated electron-hole pairs. These results can be considered promising for optoelectronic and photocatalysis applications.

Keywords: Electrodeposition; Copper(II) chloride; Copper(I) chloride; Nanorods; Photo-current

1. Introduction

Semiconductors based on nanomaterials of metal oxide have been booming over the recent decade because of the remarkable electronic and optical characteristics of these systems, which make it possible to envisage future components for micro- and nano-optoelectronics [1,2]. Among these metal oxides, the properties of zinc oxide (ZnO) are of particular interest, notably because of its non-toxicity, biocompatibility, ease of synthesis at low cost, physical and chemical stability [3], and photo-spectroscopic characteristics such as a room temperature band gap of 3.37 eV and a high exciton binding energy of 60 meV [4].

Intensive studies carried out on ZnO have led to the synthesis of various morphological structures from 1D to 3D Intensive studies conducted on ZnO have led to the synthesis of various morphological structures from 1D to 3D [5], leading to their use in numerous applications such as solar cells [6–9], photo-catalysis [10–12], photoelectrochemical (PEC) water splitting [13,14], self-cleaning surfaces [15], supercapacitor [16], sensors and biosensors [17,18]. The synthesis of ZnO is based on different manufacturing processes including sputtering [19], spray pyrolysis [20], hydrothermal [21], sol gel [22] and electrodeposition [23,24]. The latter is interesting because it is inexpensive, achievable at low temperatures, allows modulating the morphology of ZnO (thin layers or high-quality nanostructures) by adjusting the deposition parameters (potential, current density, bath temperature and precursor concentration [25]). In addition, several literature studies have confirmed that doping ZnO nanocrystals with an adequate amount of Mg, Ni, Al , Fe and Cu [26–31], modifies its electrical, magnetical and optical properties. In particular, Cu is considered an interesting dopant due to its low cost and its many chemical and physical characteristic similar to those of Zn due to the similarity of its electronic structure, leading to the replacement of Zn by Cu in the low-energy ZnO lattice [32]. The production of UV photodetection devices based on the growth of ZnO nanorods doped with different amounts of copper sulfate as a source of doping by deposition in a chemical bath has been reported, allowing to achieve a photocurrent of 3.27 mA at a bias

voltage of 5 V [33]. Another work describes the sol-gel process to elaborate Cu^{2+} doped ZnO thin films [34]. A zinc acetate bath was used as a growth medium with two different copper precursors ($Cu(CH_3COO)_2$ and $CuCl_2$) to enhance the sensing properties of ZnO nanomaterials in the propane gas atmosphere. A highest sensitivity value was recorded for the $CuCl_2$ precursor, reflecting changes in the morphology of the surface of the material, and thus a change in the adsorption energy of the contact zone.

The influence of the copper precursors ($Cu(CH_3COO)_2$ and $Cu(NO_3)_2$) was also studied on Cu-doped ZnO grown hydrothermally on a quartz substrate seeded with a ZnO layer. The nanorods doped with $Cu(CH_3COO)_2$ had better crystallization and a larger diameter than the nanorods doped with $Cu(NO_3)_2$, however, the total transmittance increased from 80% to 90% when the Cu source changed from $Cu(CH_3COO)_2$ to $Cu(NO3)_2$, respectively [35]. The growth method of ZnO and the chemical source of copper have been identified as the key issue to improve the properties of ZnO-based nanostructures. However, the majority of studies have focused on the use of copper acetate or copper nitrate as a source of dopant to form ZnO nanorods while the influence of copper chloride in the valence state (+2) has been rarely reported and, to our knowledge, no studies have been conducted previously with copper chloride in the valence state (+1).

In this work, we provide a basic understanding of how the source doping and the concentration of copper can alter the electrical properties of ZnO material prepared by electrochemical method. In general, ZnO is electrodeposited by applying a potential or a current from an aqueous medium containing zinc salts at low temperature and in the presence of OH^- anions that could be supplied from (NO_3^-), (O_2) or (H_2O_2) [36]. In this study, H_2O_2 was chosen to provide the OH^- anions and contrary to previous research, the Cu dopant from copper chloride in the form of two different valences Cu^+ and Cu^{+2} in the starting solutions was selected. A

progressive Cu doping was applied to study the optical, structural, photo-electrochemical and morphological properties of ZnO (NRs).

2. Experimental

2.1 Materials

Zinc chloride $ZnCl_2$ (Biochem, purity > 98%), potassium chloride KCl (Sigma-Aldrich, purity > 99%), hydrogen peroxide H_2O_2 (Biochem, 30%), copper(I) chloride CuCl (Sigma-Aldrich), copper(II) chloride $CuCl_2$ (Sigma-Aldrich), sodium sulfate Na_2SO_4 (Sigma-Aldrich) were used as received. ITO glass was obtained from (SOLEMS, resistivity ~ 30 Ω/square).

2.2 Preparation of samples

The electrodeposition technique was conducted with a classical cell of three electrodes using a potensiostat-galvanostat (PGSTAT204) and equipped with the NOVA software. Pure and doped ZnO nanorods were electrodeposited onto a glass substrate wrapped with transparent conductive oxide ITO (indium doped tin oxide) of an active surface area of $1cm^2$. The substrate was pre-cleaned to remove surface impurities in an ultrasonic bath, twice 10 min in acetone and ethanol and finally in diluted HNO_3 for 3 min, with rinsing with hot deionized water between each cleaning step. A platinum plaque was used as a counter electrode and a saturated calomel electrode (SCE) as reference electrode. ZnO was electrodeposited from an aqueous medium containing 0.1 M of potassium chloride (KCl), 5 mM of zinc chloride ($ZnCl_2$), and 5 mM of hydrogen peroxide (H_2O_2) [37]. Doped-ZnO samples were obtained by adding in the solution the copper salts (CuCl or $CuCl_2$). Various molar concentration ratio of ([CuCl]/[$ZnCl_2$]) and ([$CuCl_2$]/[$ZnCl_2$]) in the starting solution were tested: 0.1, 0.2, 0.5 and 1%.

The Cu-doped ZnO materials were named C_1ZnO and C_2ZnO, where C_1 indicates the presence of Cu^+ and C_2 the presence of Cu^{2+}. All samples were synthesized by potentiostatic mode by applying the voltage of -1.0 V vs. SCE for 40 min at the temperature of 70°C [38]. Double

distilled water was used to prepare the solutions and the samples were not subjected to any annealing treatment.

2.3 Characterization methods

Scanning electron microscopy (SEM) was performed on a TESCAN ,VEGA3-SBH coupled to a microscope for energy-dispersive X-ray (EDX) analyses. X-ray diffraction (XRD) patterns were collected using a MiniFlex Benchtop diffractometer with monochromatic Cu K_α radiation (λ= 1.54 Å). UV-Visible analyses were performed on a Shimadzu spectrophotometer (model UV-2300) to measure optical transmittance. XPS measurements were carried out on a Kratos Axis Ultra using AlKα (1486.6 eV) radiation. The photo-electrochemical tests were carried out with a classical cell of three electrodes: a saturated calomel electrode (SCE) as reference electrode, a platinum plaque as counter electrode and the doped-ZnO nanorods as working electrode. The three electrodes were immersed in 0.1 M Na_2SO_4 solution and the photo-response was recorded at 0.2 V_{SCE} under intermittent illumination of UV light using an ultraviolet lamp (UV Camag, 365 nm).

3. Results and discussion

3.1 Mechanism of ZnO electrodeposition

The electrochemical process for the deposition of ZnO nanostructures produced from hydrogen peroxide follows the different steps: first, H_2O_2 migrates by diffusion and is adsorbed on the working electrode (ITO), giving rise to reduction mechanisms and the formation of hydroxide ions (OH^-). Once produced, OH^- ions accumulate on the surface of the electrode, resulting in a local increase in pH. Then, on the electrode surface, the Zn^{2+} ions react with the OH^- ions to form $Zn(OH)_2$, which is unstable and evolves into ZnO as a final product at temperatures ranging from 60 to 70°C (eq.1) [39].

$$Zn^{+2} + 2OH^- \rightarrow Zn(OH)_2 \xrightarrow{70\,^\circ C} ZnO + H_2O \quad (1)$$

Copper salts can also react with OH^- ions on the surface of the electrode, but the absence of the characteristic peaks of Cu_2O or CuO in the XRD spectra (see the structural characterization) suggests that the introduction of Cu^+ or Cu^{2+} ions into the medium in the presence of Zn^{2+} ions does not noticeably change the chemical structure of ZnO. It can therefore be supposed that a minor fraction of Zn is substituted by Cu in the ZnO lattice.

3.2 Structural characterization

The crystallographic structure of ZnO, C_1ZnO and C_2ZnO was investigated by X-ray diffraction recorded from 20° to 80° (in 2θ). In Fig.1(a,b), all the diffraction peaks are narrow and sharp, which means a good crystallization, and can be indexed to hexagonal Würtzite structure of zinc oxide (JCPDS card No. 01-080-0074). The XRD shows a preferential orientation along the (002) plane suggesting that the crystalline grains are mainly oriented along the c-axis. The appearance of low-intensity peaks for pure ZnO has been referred to (100), (101) and (103) planes at $2\theta = 31.82^{\circ}$, 36.30° and 62.89°, respectively. In addition, no peaks related to any another copper or zinc phases (i.e. no impurities) are observed, indicating that the concentration of the dopants are below the solubility limit.

The intensity of C_1ZnO and C_2ZnO peaks decreases with increasing Cu concentration and this decrease is greater for C_2ZnO than for C_1ZnO. This can be explained by the ionic radius of Cu^{2+} (71 p.m), which is slightly smaller than that of Cu^+ (73 p.m) and close to that of Zn^{2+} (74 p.m) [40,41]. The substitution of Zn^{2+} in the ZnO lattice with Cu^{2+} ions creates shorter bonds than in the presence of Cu^+ ions, which can degrade the quality of the crystal. In addition, in the presence of Cu^{2+}, the peak position of (002) plane shifts to higher angles (Fig 1a). According to P.Jongnavakit et al. [42], the replacement of Zn^{2+} by Cu^{2+} ions shifts the peaks to higher angles, which confirms our observation. However, for C_1ZnO, the peak position of (002) plane moves toward lower angles values when the Cu^+ concentration is increased (Fig 1b). In general,

the XRD spectra obtained for C_1ZnO and C_2ZnO are quite similar to those reported in previous researches [29,41]. We believe that the oxidation state (+1 or +2) of the Cu ions in the ZnO lattice is responsible for the discrepancy in the above findings.

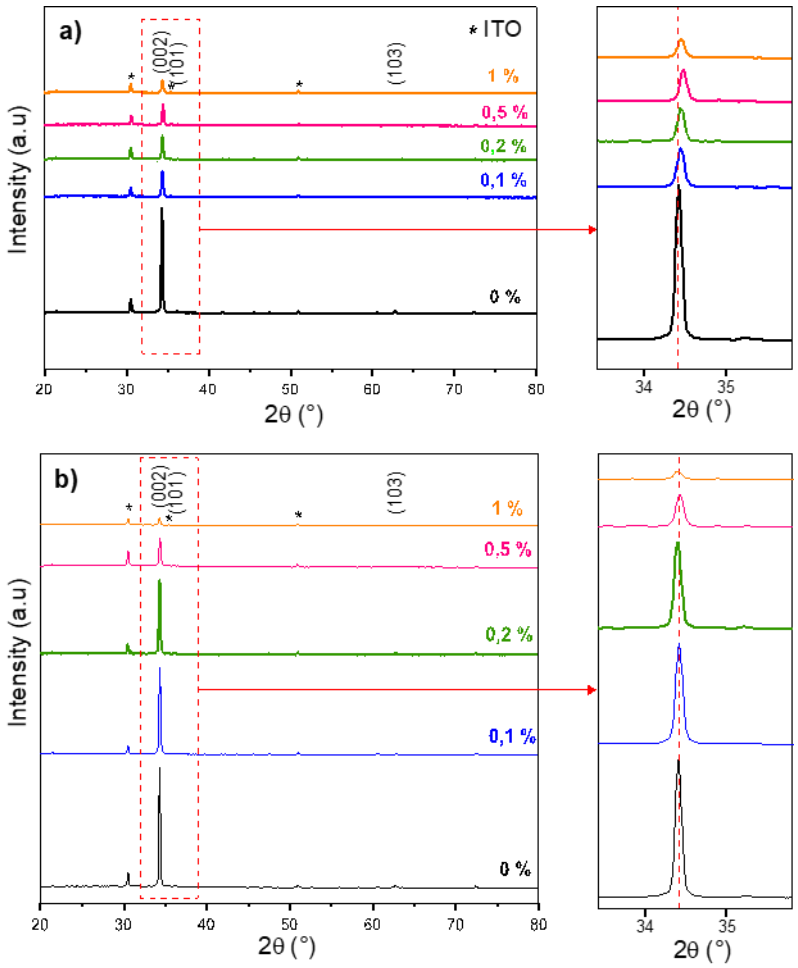

Fig. 1. XRD patterns: a) C_2ZnO and b) C_1ZnO for different molar concentration ratio: 0, 0.1, 0.2, 0.5 and 1%

In order to properly understand the effect of doping by Cu^+ and Cu^{2+} on the structure of ZnO (NRs), we have estimated the lattice parameters, a and c, from the (002) and (100) peaks of ZnO, using the equation (2) [43], where d is the inter-planer spacing (in Å), *h* , *k* and *l* are the miller indices:

$$2d \sin\theta = n\lambda \ \ and \ d^2 = \left[\frac{4}{3}\left(\frac{h^2+hk+k^2}{a^2}\right)+\frac{l^2}{c^2}\right]^{-1} \qquad (2)$$

From Table 1, the lattice parameters of pure ZnO were estimated to be *a* = 3.007 Å and *c* = 5.2083 Å. For the C_2ZnO samples, both parameters decreased with the increase of Cu^{2+} concentration compared with pure ZnO, the shortening in the c-axis proving the substitution of Cu^{2+} by Zn^{2+} at the Zn sites in the ZnO lattice. Our observation is similar to the result obtained by F.Ghahramanifard et al. [40], where *a* and *c* parameters decreased with increasing Cu^{2+} content up to 0.5%. When CuCl was used as Cu precursor instead of $CuCl_2$, the lattice parameters value changed slightly as the Cu^{+} content increases. The difference in the lattice parameters between C_2ZnO and C_1ZnO samples can be assigned to the existence of micro-strains and lattice defects in the crystal and the small difference in ion radius size between Cu^{+} and Cu^{2+}. According to the literature [44], an ideal ZnO structure has a ratio (c/a) between 1.593 to 1.603. Our results are slightly higher with a ratio of 1.732, which indicates that Cu^{+} or Cu^{+2} does not caused considerable distortion in the hexagonal structure of ZnO wurtzite. To determine the crystallite size of ZnO, C_1ZnO and C_2ZnO samples, the Scherrer equation (eq. 3) was applied [41]:

$$D = \frac{0.9\,\lambda}{\beta\, cos\theta_{(002)}} \qquad (3)$$

Where λ is the X-ray wavelength, β is the full width at half maximum (FWHM) in radians and θ is the Bragg's angle.

As shown in table 1 and fig. 2, the decrease in crystallite size with Cu doping is due to the appearance of new small crystallites. This is explained by the Zener theory [45], which accepts that the introduction of copper ions into the host ZnO crystal acts as an obstacle preventing both grain movement and crystal growth. Finally, to identify the state of stress of the samples, the strain ε (along the c-axis) and the residual stress σ (parallel to the layer surface) were calculated from (eq. 4 and 5) [32,40]:

$$\varepsilon\ (\%) = \frac{C - C_0}{C_0} \times 100 \qquad (4)$$

$$\sigma\ (Gpa) = -\ 233 \times \varepsilon \qquad (5)$$

Where c is the lattice parameter of the electrodeposited layer and c_0 is the lattice parameter of the standard ZnO powder (c_0 = 0.5215 nm).

As observed in Table1, the negative sign of ε values indicates that the ZnO layer is under a compressive strain along the c axis, whereas, the positive sign of the σ values indicates that the nanostructures are subjected to tensile stress perpendicular to the c-axis. Besides, it is worthy to note that the incorporation of copper in ZnO lattice affects the stress state, which, in turn, affects the position of the peak as discussed previously [46,47].

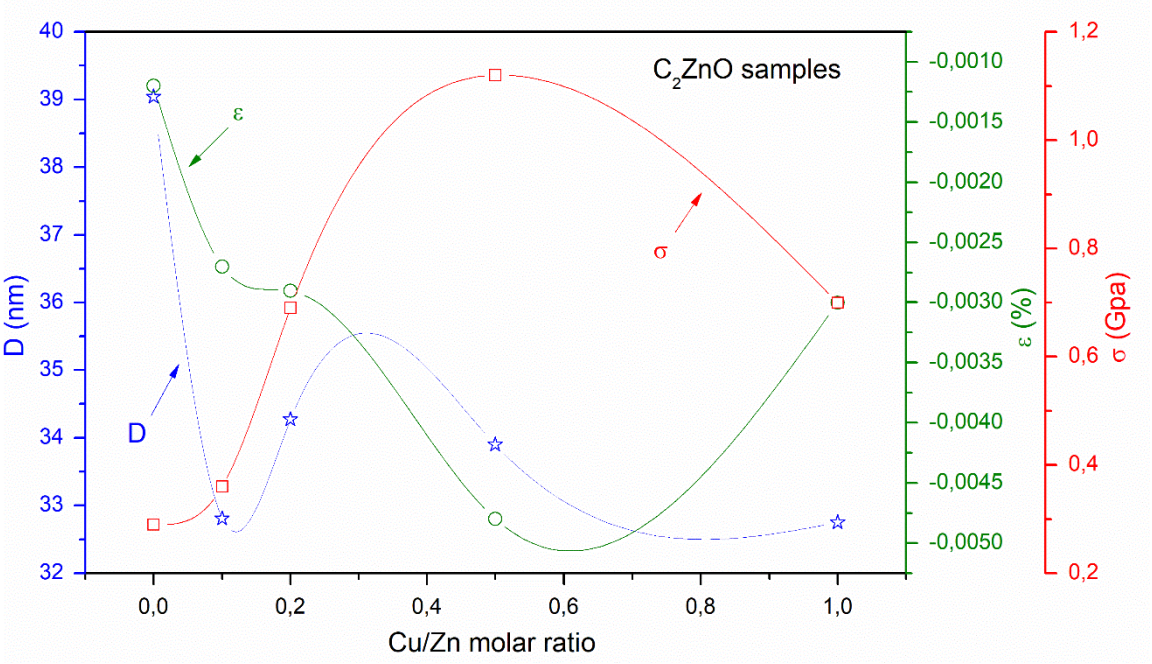

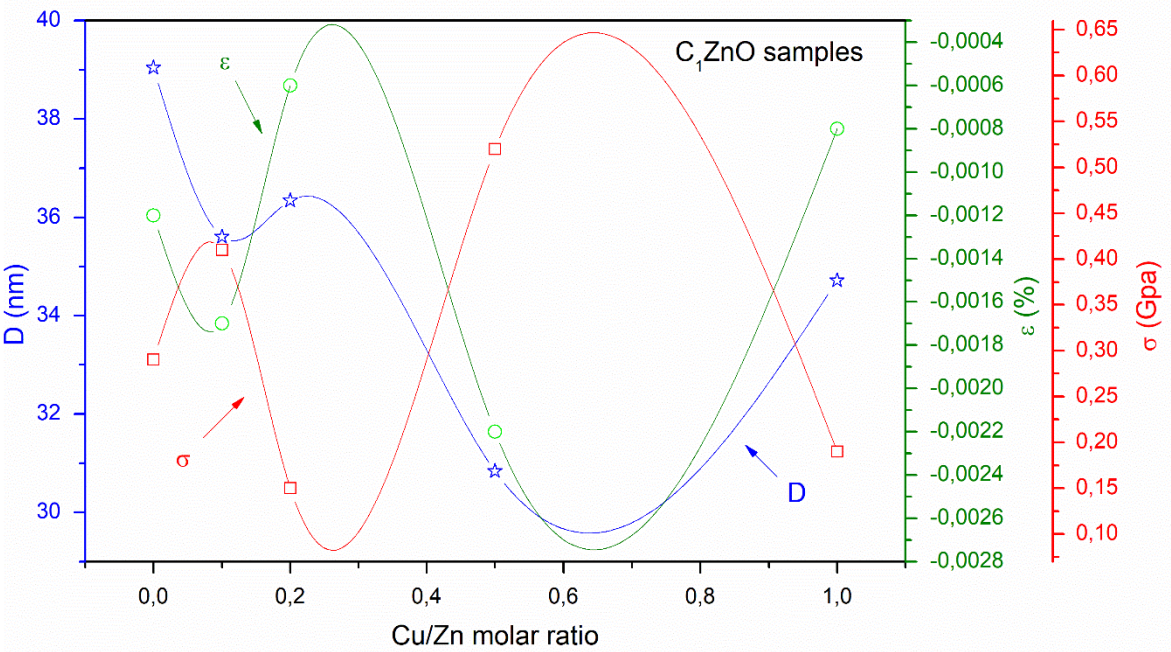

Fig. 2. Variations of crystallite size (D), strain (ε) and stress (σ) for: **a)** C_2ZnO and **b)** C_1ZnO for different copper content: 0, 0.1, 0.2, 0.5 and 1%.

Table 1. Crystal data extracted from the XRD diagrams of pure ZnO, and ZnO doped with Cu^+ and Cu^{2+} for different molar concentration ratios: 0, 0.1, 0.2, 0.5 and 1%.

Sample	**2θ (°) (002)**	**Lattice parameters**		**c/a ratio**	**D (nm)**	**ε (%)**	**σ (Gpa)**
		a=b [Å]	**c [Å]**				
Pure ZnO (0%)	34,410	3,007	5,208	1,7319	39,04	-0,0012	0,29
0.1% C_2ZnO	34,462	3,002	5,200	1,7321	32,81	-0,0027	0,63
0.2% C_2ZnO	34,471	3,001	5,199	1,7324	34,27	-0,0029	0,69
0.5% C_2ZnO	34,536	2,996	5,189	1,7319	33,9	-0,0048	1,12
1% C_2ZnO	34,473	3,001	5,199	1,7324	32,75	-0,0030	0,70
0.1% C_1ZnO	34,428	3,005	5,205	1,7321	35,61	-0,0017	0,41
0.2% C_1ZnO	34,388	3,008	5,211	1,7323	36,34	-0,0006	0,15
0.5% C_1ZnO	34,445	3,004	5,203	1,7320	30,84	-0,0022	0,52
1% C_1ZnO	34,394	3,008	5,210	1,7320	34,72	-0,0008	0,19

3.3 Morphological characterization

The morphology in top view of the ZnO, C_1ZnO and C_2ZnO samples is showed in Fig. 3. The ZnO material obtained without Cu doping appears as a flat surface consisting of uniform and closed hexagonal nanorods packed against each other. For C_2ZnO, with the increase in the Cu^{2+} concentration in the ZnO lattice, the shape of the nanorods changes: at 0.1% Cu, the size of the nanorods becomes smaller, then the nanostructures coalesce at 0.2% Cu^{2+} and some of them overlapped with each other, manifesting themselves on the surface as a flower-like structure. Srinivasan [48] has clarified this phenomenon as a result of the increased surface energy of ZnO in the presence of impurities, which give rise to the development of nano-flowers. At 0.5 and 1% Cu^{2+}, other structures begin to appear with a deterioration of the majority of the hexagonal rods and a random distribution of their diameter between 134 and 308 nm.

For C_1ZnO, the effect of ZnO doping with Cu^{+} results in a different evolution of the material. Up to 0.2% Cu^{2+}, a higher density of smaller diameter nanorods is observed, and from 0.5% Cu^{+}, the diameter of the nanorods appears to increase slightly, giving rise to popcorn-like structures in the presence of 1% Cu^{+}. This result is in agreement with our observations from the previous XDR analyses, which showed a deformation of the lattice parameters with the presence of Cu in ZnO. The number of the ZnO nanorods per unit area (density) obtained is of the order of 7×10^{8} NRs/cm^2 while the nanorods density is 8×10^{8}NRs/cm^2 for arrays doped with 0.5 % of Cu^{2+} and 9×10^{8}NRs/cm^2 for those doped with 0.1% of Cu^{+}.

It is interesting to note that the growth medium of ZnO is sensitive to compositional changes. Consequently, the incorporation of Cu^{+} or Cu^{2+} ions modifies the growth procedure of the nanorods which act as defects in the ZnO host lattice [49].

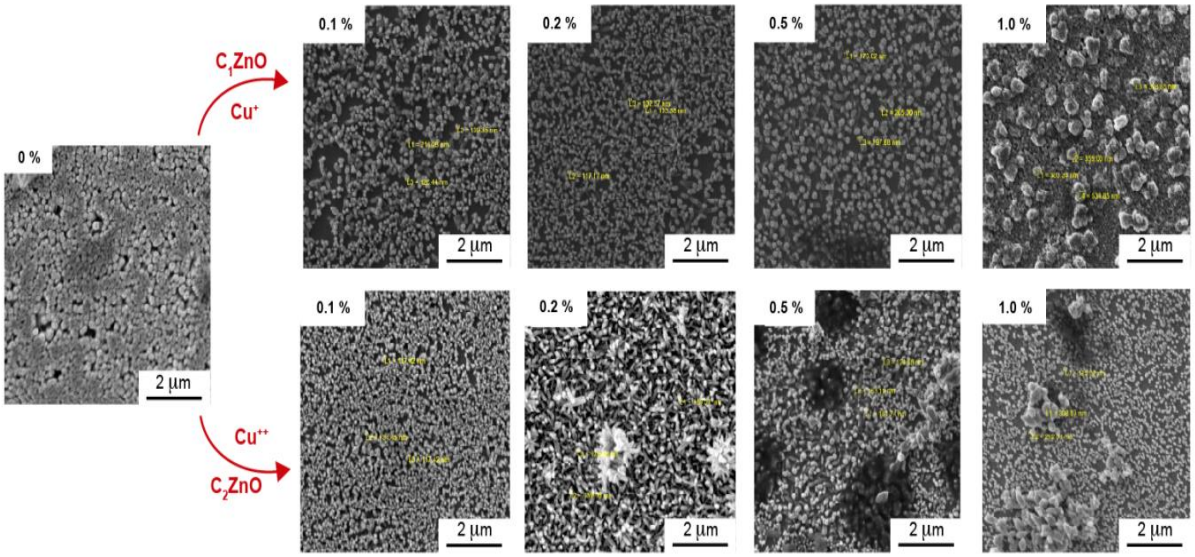

Fig. 3. Top view SEM images for ZnO, C_1ZnO and C_2ZnO for different molar concentration ratio: 0, 0.1, 0.2, 0.5 and 1%

A qualitative analysis for C_1ZnO, C_2ZnO and ZnO samples was performed by EDS analysis. From Fig. 3, for undoped ZnO, the existence of both Zn and O elements confirms the formation of ZnO structures. After doping, the presence of Cu indicates the successful integration of Cu into the ZnO lattice. As expected, the percentage of Cu increases with the increasing in $CuCl_2$ and CuCl salts in solution. The higher Cu content observed in the ZnO lattice that was obtained from the CuCl salt can be explained by the release of a lower amount of Cl^- anions, which adsorbed on the surface of the electrode and thus slowed down the ZnO (NRs) deposition mechanism. The EDS analysis does not reveal the presence of other peaks from possible impurities, and the findings are in good agreement with those obtained by X-ray diffraction.

Table 2. Cu content in the initial medium and in samples detected by EDS.

Sample	Initial Cu concentration (µmol)	Molar concentration ratio (Cu salt/Zn salt)	Atomic Cu content measured by EDS (at.%)
CuCl	5	0.1	0.04
	10	0.2	0.14
	25	0.5	0.28
	50	1	0.87
$CuCl_2$	5	0.1	0.02
	10	0.2	0.09
	25	0.5	0.10
	50	1	0.13

3.4 Optical properties

The influence of Cu doping on the transmission and on the band gap of the samples was studied by UV-Visible spectrophotometry. From Fig. 4, it is clear that both C_1ZnO and C_2ZnO exhibit a red shift of the absorption edge compared to ZnO. This observation can be taken as an indicator for the decrease of the optical band gap [32]. According to Fig. 4a, the transmission value increases from 77.46 for ZnO to the maximum value of 96.13% for C_2ZnO (doped with 0.1% Cu^{2+}). This trend has also been observed by Kumaresan *et* al. for the doping of ZnO with copper and aluminum. For C_1ZnO samples (Fig. 4b), we observe two trends: first, the transmission value increases to the maximum value of 86.03% for ZnO doped with 0.2% Cu^{+}, and second, the transmittance value drops sharply to 51% for ZnO doped with 1% Cu^{+}. The increase in transmission can be explained by the formation of a thin layer of electrodeposited nanorods on the electrode, while a thicker layer of electrodeposited nanorods results in lower transmission. The highest transmission values are obtained for C_2ZnO, which can therefore be considered a preferable material to C_1ZnO for electro-optical UV applications and solar cells, as they require the use of materials with high optical transparency and electron conduction properties. However, the lower transmittance of C_1ZnO (doped with 1% Cu^{+}) indicates that this

material has a higher absorbance in the visible region, which is preferable for photocatalytic applications using visible light. The band-gap energy (E_g) can be estimated using the following equation [49]:

$$\alpha h\nu = A\,(h\nu - E_g)^n \qquad (6)$$

Where α is the absorption coefficient, $h\nu$ is the photon energy, E_g is optical band gap and the exponent n is equals to (1/2) in our case.

To verify the optical band gap reduction, we plotted the variation of $(\alpha h\upsilon)^2$ as a function of $(h\upsilon)$ as shown in Fig. 5. The band-gap energy (E_g) of ZnO, C_1ZnO and C_2ZnO is determined from the extrapolation of the linear part with the $h\upsilon$ axis for $(\alpha h\upsilon)^2 = 0$. The E_g value of ZnO (NRs) is about 3.36 eV, which is almost the same of ZnO in the massive form 3.37 eV [4]. However, when Cu content increases from 0.1 to 1% in ZnO, E_g decreases from 3.20 to 3.06 eV for C_2ZnO, and from 3.34 to 3.02 eV for C_1ZnO (Fig. 5c). The decrease in E_g has also been observed by other authors when doping ZnO with Cu [29,41], and is explained by the exchange interactions at the p-d orbitals (3d Zn and 2p O to 3d Cu and 2p O) during the introduction of copper ions in the ZnO lattice [46,50,51]. Additionally, the significant difference in electro-negativity between Zn (1.65) and Cu (1.95) atoms may also be a reason for the reduction of the band-gap [52].

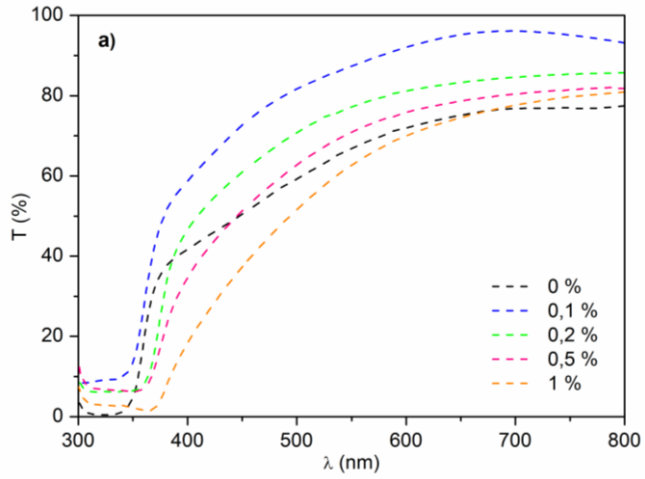

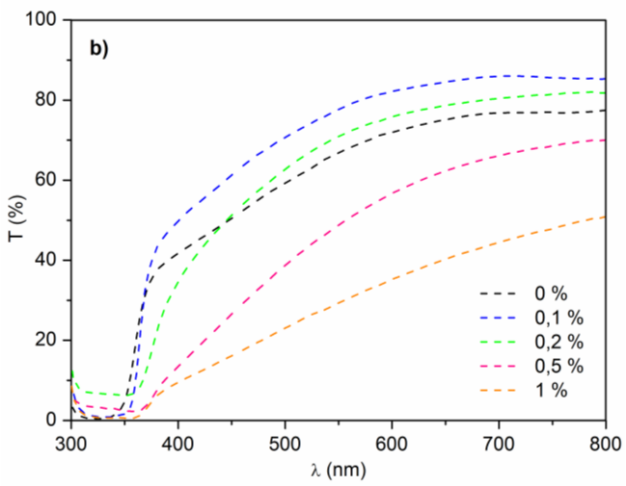

Fig. 4. Transmittance spectra of Cu-doped ZnO for **a)** C_2ZnO and **b)** C_1ZnO for different molar concentration ratio: 0, 0.1, 0.2, 0.5 and 1%

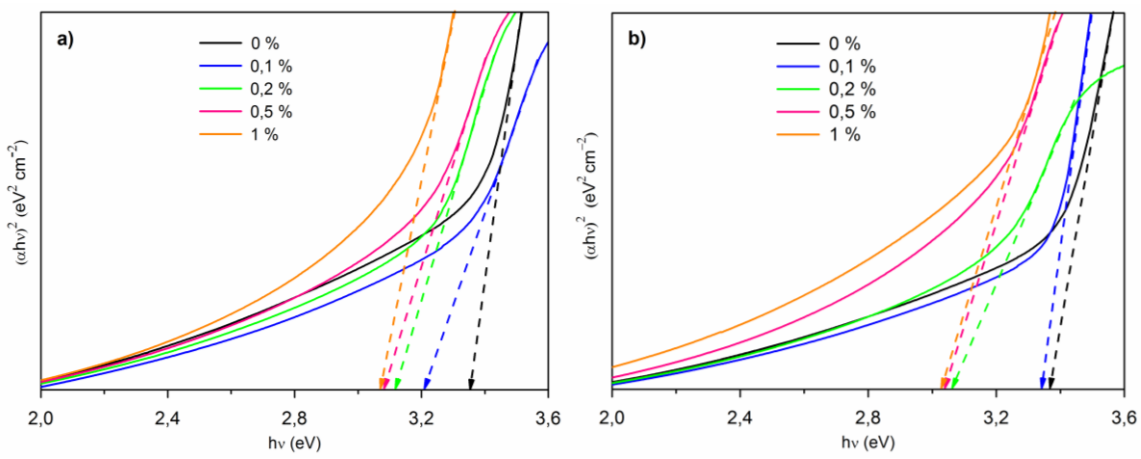

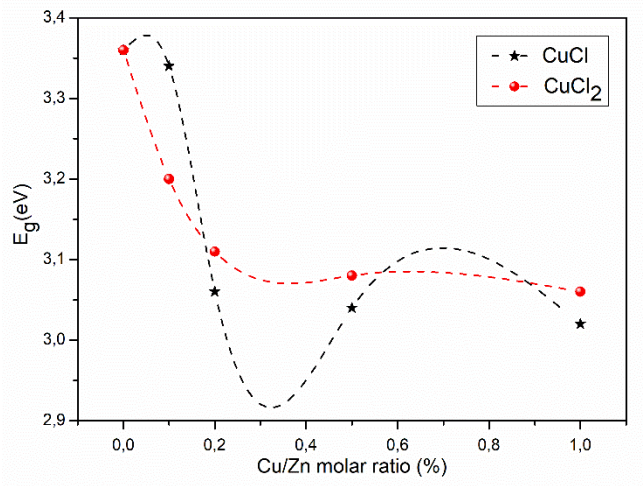

Fig. 5. Band gap energy plot for **a)** C_2ZnO**, b)** C_1ZnO for different molar concentration ratio: 0, 0.1, 0.2, 0.5 and 1%**, c)** E_g Vs. CuCl and $CuCl_2$ content.

3.5 XPS analysis

To determine the presence of Cu in the doped samples, X-ray photoelectron spectroscopy (XPS) measurements were performed on the samples 0.1% C_1ZnO, 0.5% C_2ZnO, and pure ZnO, based on the best results obtained for the photoelectrochemical tests. From the survey spectrum in Fig. 6a, the peaks are attributed to the Zn, C, O elements, and additional peaks characteristic of Cu 2p are observed at around 965 eV, confirming the presence of Cu element in the samples C_1ZnO and C_2ZnO. The presence of carbon is caused by the inevitable air exposure when the sample is placed into the XPS chamber. Fig. 6b shows the Zn 2p spectra of C_1ZnO, C_2ZnO, and pure ZnO samples. The binding energies at 1020.7 and 1043.7 eV are related to Zn $2p_{3/2}$ and Zn $2p_{1/2}$ lines, respectively. The distance between the peaks Zn $2p_{3/2}$ and Zn $2p_{1/2}$ is 23.1 eV, reflecting the oxidation state of Zn^{2+} in ZnO [53]. After doping, the peaks slightly shift toward a higher binding energy, suggesting that Cu^{2+} and Cu^{+} have substituted Zn^{2+} in the ZnO lattice [54,55]. Figs. 6c,e present the O 1s spectrum of C_2ZnO and C_1ZnO samples. The peak is splitted into three peaks. The peak ~530 eV corresponds to the oxygen O^{2-} in the crystal lattice linked to Zn^{2+}, forming the O–Zn bonds. The peaks at ~531 eV corresponds to the adsorbed oxygen, while the peak at ~532 eV can be attributed to the presence of both hydroxyl groups and a small amount of water molecules in the ZnO lattice.

Fig. 6d displays the Cu 2p spectrum of C_2ZnO, where two peaks are detected at 952.2 and 932.4 eV that correspond to the electronic configurations of Cu $2p_{3/2}$ and Cu $2p_{1/2}$, respectively, confirming that Cu is in a divalent valence state (Cu^{2+}) [55]. For C_1ZnO, in Fig. 6f, the two electronic configurations of Cu are located at 952.4 and 932.6 eV, respectively

[17,54]. Based on the XPS results, it is evident that Cu exists in the cationic state Cu^{2+} or Cu^{+} in the materials as a result of a partial replacement of a fraction of the Zn^{2+} sites in ZnO.

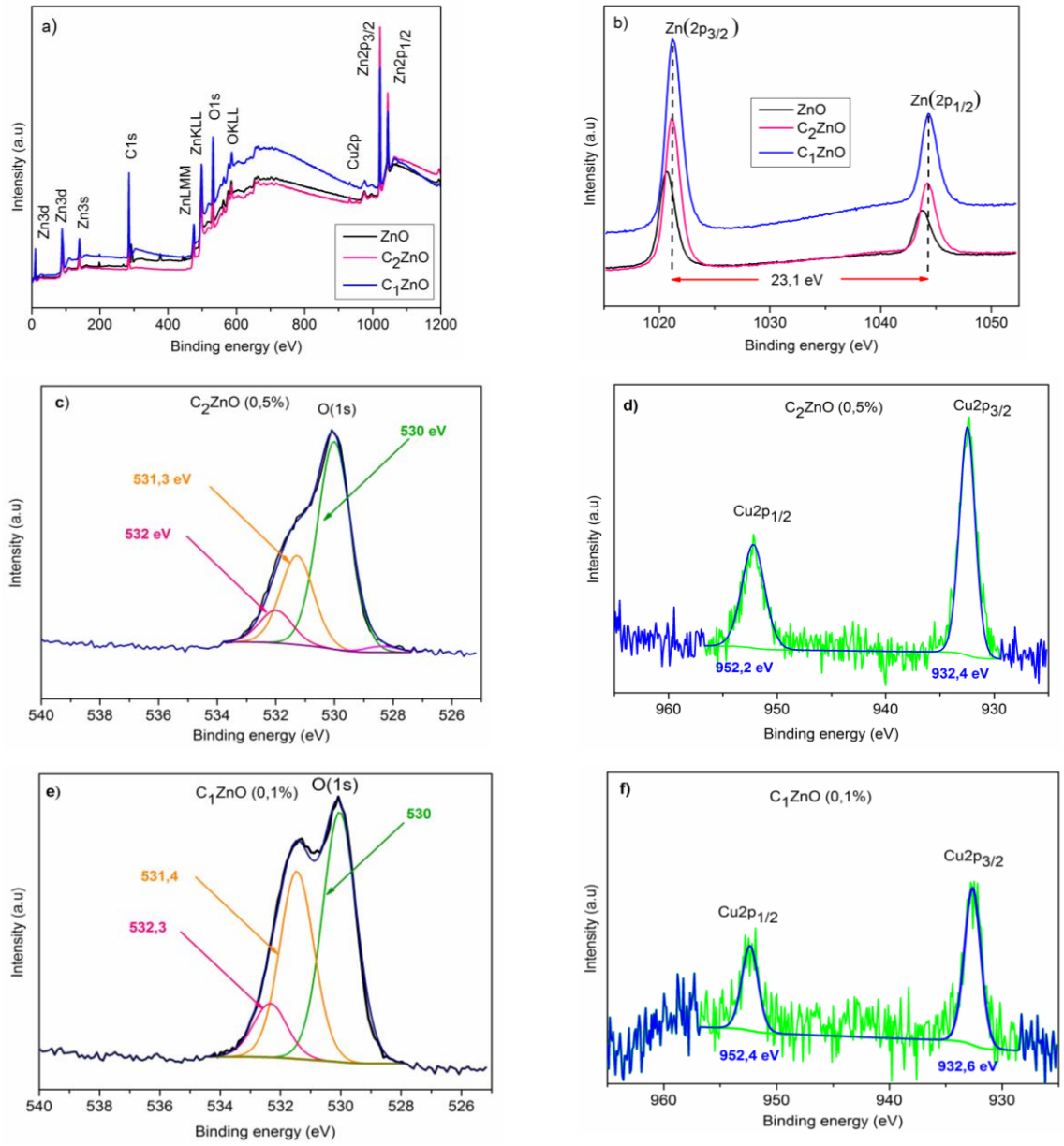

Fig. 6. X-ray photoelectron spectroscopy (XPS) of ZnO, 0.5% C_2ZnO and 0.1% C_1ZnO nanorods.

3.6 Photoelectrochemical tests

When a semiconductor is exposed to photons of a wavelength exceeding its interval, it generates electron-hole pairs (e^-,h^+) at the point of radiation absorption. Photoelectroactivity tests were carried out by chronoamperometry in a 0.1 M Na_2SO_4 medium for pure and Cu-doped ZnO samples. The change in current density was recorded over time under intermittent UV light (every 5 seconds) and an imposed potential (E = 0.2 V_{SCE}). The results are shown in Fig. 7. In the dark, the photocurrent of all samples decreases quite rapidly until the electrode equilibrium is restored. However, under UV illumination (365 nm), an important increase in current density is observed for C_1ZnO and C_2ZnO. For pure ZnO, the photocurrent density is about 0.004 mA.cm^{-2}, while for C_2ZnO samples (Fig. 7a), the photocurrent response increases to the maximum value of 0.05 mA.cm^{-2} when the molar concentration ratio reaches 0.5% and then decreases to 0.016 mA.cm^{-2} for 1%. In contrast, the photocurrent density of C_1ZnO (Fig. 7b) reaches 0.04 mA.cm^{-2} at the molar concentration ratio 0.1%, and then gradually decreases to 0.01 mA.cm^{-2} for 1%. Compared to pure ZnO, the improvement is 10 times greater for C_1ZnO while it is 12 times greater for C_2ZnO. The drop in the photo-current response at the molar concentration ration of 1% could be caused by the high amount of Cu incorporated in the host lattice, which might act as a deep electron trap and thus degrade the photo-activity of the resulting material [28]. As we mentioned earlier, when a semiconductor is exposed to photons of a wavelength exceeding its band-gap energy, electrons in the valence band (VB) migrate to the conduction band (CB) of the semiconductor material, leaving behind holes in the valence band. For pure ZnO, the electrons return to the VB from the CB, however, in the presence of Cu, the electrons from the conduction band are rather recovered by the Cu^{2+} level, inducing the reduction of Cu^{2+} to Cu^+, and thus creating defect levels (Cu^{2+}-Cu^+) in the mid gap of ZnO. The lifetime of the photogenerated carriers is extended and the electron-hole pairs are effectively

separated [49]. All electrodeposited ZnO films exhibited an anodic photo-current density, characteristic of a n-type semiconductor [26].

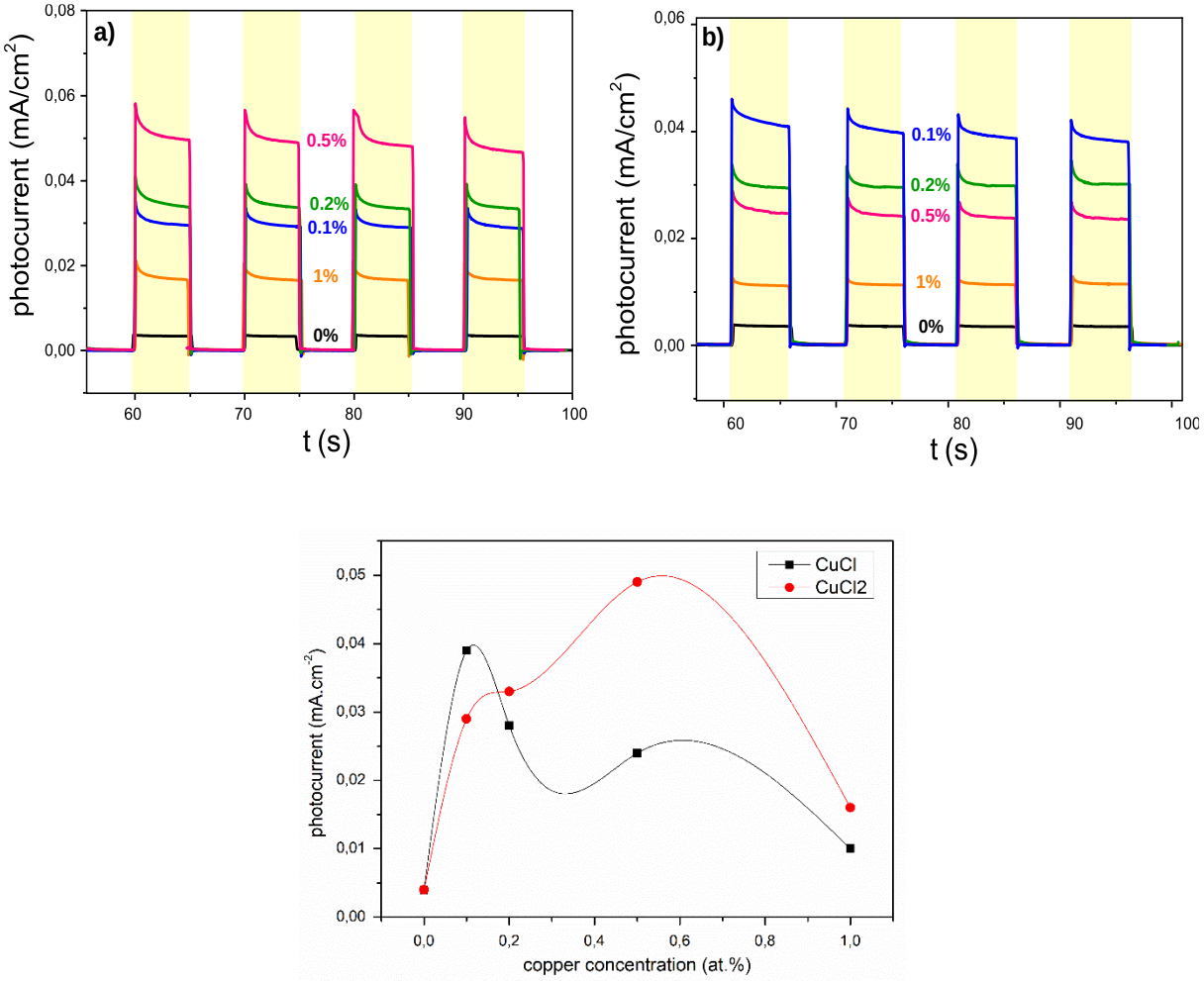

Fig. 7. Photocurrent-time response of **a)** C_2ZnO, **b)** C_1ZnO, **c)** photocurrent density *vs* CuCl and $CuCl_2$ content.

4. Conclusion

In this work, we explored the effect of $CuCl_2$ and CuCl doping on the morphological, optical and structural properties of ZnO (NRs) using an easy electrochemical deposition technique. The XRD results show that the introduction of Cu^{+} or Cu^{2+} ions induce defects in the ZnO host lattice, leading to the deformation of the ZnO crystal lattice. This phenomenon is corroborated by SEM observations, which show changes in the morphology of the nanostructures after Cu doping. According to optical measurements, both C_1ZnO and C_2ZnO samples display a redshift in the visible light region as the Cu content increases, which indicates a reduction in the optical band gap of ZnO. Lastly, in the presence of Cu dopant, photoelectrochemical tests under UV illumination (365 nm) show current densities of 0.04 $mA.cm^{-2}$ and 0.05 $mA.cm^{-2}$ for C_1ZnO and C_2ZnO, respectively, ten to twelve times superior to that of pure ZnO nanorods (0.004 $mA.cm^{-2}$). The increased photoelectrochemical activity of the doped ZnO (NRs) has been attributed to the narrowing of the band gap induced by the introduction of defects level in the mid-gap of ZnO lattice. C_2ZnO samples characterized by a high transmittance and improved photo-current can be considered a preferable material for electro-optical UV applications and thin film based solar cells, as they require the use of materials with high optical transparency and electron conduction properties. However, the lower transmittance of the C_1ZnO samples (especially doped with 1% Cu^{+}) might be preferable for photocatalytic applications using visible light.

References

[1] Y. Bouznit, A. Henni, Characterization of Sb doped SnO2 films prepared by spray technique and their application to photocurrent generation, Mater. Chem. Phys. 233 (2019) 242–248. doi:10.1016/j.matchemphys.2019.05.072.

[2] W. Rakhrour, D. Selloum, A. Henni, N. Cherrad, I. Chikouche, M. Benalia, S. Mouffok, M. Djedid, N. Bouzar, S. Tingry, Electrochemical Synthesis of an Organometallic Material Based on Polypyrrole/MnO2 as High-Performance Cathode, J. Inorg. Organomet. Polym. Mater. 31 (2021) 62–69. doi:10.1007/s10904-020-01664-w.

[3] Ü. Özgür, Y.I. Alivov, C. Liu, A. Teke, M.A. Reshchikov, S. Doğan, V. Avrutin, S.J. Cho, H. Morkọ, A comprehensive review of ZnO materials and devices, J. Appl. Phys. 98 (2005) 1–103. doi:10.1063/1.1992666.

[4] C. Klingshirn, ZnO: From basics towards applications, Phys. Status Solidi Basic Res. 244 (2007) 3027–3073. doi:10.1002/pssb.200743072.

[5] N. Saravanan, R. Eric, Photocatalysts, n.d.

[6] E. Praveen, I.J. Peter, A.M. Kumar, K. Ramachandran, K. Jayakumar, Boosting of Power Conversion Efficiency of 2D ZnO Nanostructures-Based DSSC by the Lorentz Force with Chitosan Polymer Electrolyte, J. Inorg. Organomet. Polym. Mater. (2020). doi:10.1007/s10904-020-01629-z.

[7] D.V. Pandi, V. Saraswathi, N. Muthukumarasamy, S. Agilan, P. Balraju, D. Velauthapillai, C-axis oriented ZnO nanorods based quantum dot solar cells, Opt. Mater. (Amst). 112 (2021) 110774.

[8] R. Singh, R.B. Choudhary, Ag/AgCl sensitized n-type ZnO and p-type PANI composite as an active layer for hybrid solar cell application, Optik (Stuttg). 225 (2021) 165766.

[9] R. Alfanaar, P.E. Elim, Y. Yuniati, H.S. Kusuma, M. Mahfud, Synthesis of TiO2/ZnO-Anthocyanin Hybrid Material for Dye Sensitized Solar Cell (DSSC), in: IOP Conf. Ser. Mater. Sci. Eng., IOP Publishing, 2021: p. 12088.

[10] K.H. Park, G.D. Han, B.J. Kim, E.H. Kang, J.S. Park, J.H. Shim, H.D. Park, Effects of

atomic layer deposition conditions on the formation of thin ZnO films and their photocatalytic characteristics, Ceram. Int. 45 (2019) 18823–18830. doi:10.1016/j.ceramint.2019.06.115.

[11] C. Shi, L. Zhang, H. Bian, Z. Shi, J. Ma, Z. Wang, Construction of Ag–ZnO/cellulose nanocomposites via tunable cellulose size for improving photocatalytic performance, J. Clean. Prod. 288 (2021) 125089.

[12] A.M. Ramesh, S. Shivanna, Hydrothermal synthesis of MoO3/ZnO heterostructure with highly enhanced photocatalysis and their environmental interest, J. Environ. Chem. Eng. 9 (2021) 105040.

[13] K.E. Salem, A.M. Mokhtar, I. Soliman, M. Ramadan, B.S. Shaheen, N.K. Allam, Ge-doped ZnO nanorods grown on FTO for photoelectrochemical water splitting with exceptional photoconversion efficiency, Int. J. Hydrogen Energy. 46 (2021) 209–220. doi:10.1016/j.ijhydene.2020.09.208.

[14] S. Swathi, R. Yuvakkumar, G. Ravi, E.S. Babu, D. Velauthapillai, S.A. Alharbi, Morphological exploration of chemical vapor–deposited P-doped ZnO nanorods for efficient photoelectrochemical water splitting, Ceram. Int. 47 (2021) 6521–6527.

[15] Y.S. Wy, N. Johari, S.A. Mazlan, N.A. Hassan, Mechanochemical durability and self-cleaning performance of zinc oxide-epoxy superhydrophobic coating prepared via a facile one-step approach, Ceram. Int. (2021).

[16] C. Paraschiv, G. Hristea, M. Iordoc, B.-G. Sbarcea, V. Marinescu, Hydrothermal growth of ZnO/GO hybrid as an efficient electrode material for supercapacitor applications, Scr. Mater. 195 (2021) 113708.

[17] O. Alev, N. Sarıca, O. Özdemir, L.Ç. Arslan, S. Büyükköse, Z.Z. Öztürk, Cu-doped ZnO nanorods based QCM sensor for hazardous gases, J. Alloys Compd. 826 (2020) 154177. doi:10.1016/j.jallcom.2020.154177.

[18] S. Chakraborty, R. Saha, A. Karmakar, S. Chattopadhyay, Fabrication and Characterization of Zinc Oxide Nanowire Based Two-electrode Capacitive Biosensors on Flexible Substrates for Estimating Glucose Content in a Sample, Electroanalysis. (2021).

[19] J. Soudi, K.M. Sandeep, B.K. Sarojini, P.S. Patil, S.R. Maidur, K.M. Balakrishna, Thermo-optic effects mediated self focusing mechanism and optical power limiting studies of ZnO thin films deposited on ITO coated PET substrates by RF magnetron sputtering under continuous wave laser regime, Optik (Stuttg). 225 (2021) 165835.

[20] Y. Bouznit, A. Henni, Enhanced photoelectrochemical performance of Al-doped ZnO thin films prepared by co-spray technique, Mater. Sci. Semicond. Process. 118 (2020) 105208. doi:10.1016/j.mssp.2020.105208.

[21] A. Phuruangrat, B. Kuntalue, S. Thongtem, T. Thongtem, Hydrothermal synthesis of hexagonal ZnO nanoplates used for photodegradation of methylene blue, Optik (Stuttg). 226 (2021) 165949.

[22] A. Mahroug, B. Mari, M. Mollar, I. Boudjadar, L. Guerbous, A. Henni, N. Selmi, Studies on structural, surface morphological, optical, luminescence and Uv photodetection properties of sol–gel Mg-doped ZnO thin films, Surf. Rev. Lett. (2018) 1850167. doi:10.1142/S0218625X18501676.

[23] I.L. Ikhioya, N.I. Akpu, A.C. Nkele, Influence of ytterbium (Yb) dopant on the optical properties of electrochemically deposited zinc oxide (ZnO) films, Mater. Res. Express. 8 (2021) 16403.

[24] A. Henni, N. Harfouche, A. Karar, D. Zerrouki, F.X. Perrin, F. Rosei, Synthesis of graphene–ZnO nanocomposites by a one-step electrochemical deposition for efficient photocatalytic degradation of organic pollutant, Solid State Sci. 98 (2019) 106039. doi:10.1016/j.solidstatesciences.2019.106039.

[25] M.R. Khelladi, L. Mentar, A. Beniaiche, L. Makhloufi, A. Azizi, A study on electrodeposited zinc oxide nanostructures, J. Mater. Sci. Mater. Electron. 24 (2013) 153–159. doi:10.1007/s10854-012-0973-5.

[26] A. Henni, A. Merrouche, L. Telli, A. Karar, Studies on the structural, morphological, optical and electrical properties of Al-doped ZnO nanorods prepared by electrochemical deposition, J. Electroanal. Chem. 763 (2016) 149–154. doi:10.1016/j.jelechem.2015.12.037.

[27] D. Selloum, A. Henni, A. Karar, A. Tabchouche, N. Harfouche, O. Bacha, S. Tingry, F. Rosei, Effects of Fe concentration on properties of ZnO nanostructures and their

application to photocurrent generation, Solid State Sci. 92 (2019) 76–80. doi:10.1016/j.solidstatesciences.2019.03.006.

[28] F. Rasouli, A. Rouhollahi, F. Ghahramanifard, Gradient doping of copper in ZnO nanorod photoanode by electrodeposition for enhanced charge separation in photoelectrochemical water splitting, Superlattices Microstruct. 125 (2019) 177–189. doi:10.1016/j.spmi.2018.08.026.

[29] A. Gaurav, R. Beura, J.S. Kumar, P. Thangadurai, Study on the effect of copper ion doping in zinc oxide nanomaterials for photocatalytic applications, Mater. Chem. Phys. 230 (2019) 162–171. doi:10.1016/j.matchemphys.2019.03.056.

[30] M. Sajjadnejad, S.M.S. Haghshenas, V.T. Targhi, N. Setoudeh, A. Hadipour, A. Moghanian, S. Hosseinpour, Wear behavior of alkaline pulsed electrodeposited nickel composite coatings reinforced by ZnO nanoparticles, Wear. 468 (2021) 203591.

[31] S. Rajpal, S. Kumar, S.R. Kumar, POST ANNEALING ANALYSIS OF Mg DOPED ZnO THIN FILMS DEVELOPED BY ELECTRODEPOSITION TECHNIQUE, AIJR Abstr. (2021) 142.

[32] A.M. El Sayed, G. Said, S. Taha, A. Ibrahim, F. Yakuphanoglu, Influence of copper incorporation on the structural and optical properties of ZnO nanostructured thin films, Superlattices Microstruct. 62 (2013) 47–58. doi:10.1016/j.spmi.2013.07.005.

[33] R. Shabannia, A high photocurrent gain in UV photodetector based on Cu doped ZnO nanorods on PEN substrate, J. Mater. Sci. Mater. Electron. 29 (2018) 11646–11652. doi:10.1007/s10854-018-9262-2.

[34] H. Gómez-Pozos, E.J.L. Arredondo, A.M. Álvarez, R. Biswal, Y. Kudriavtsev, J.V. Pérez, Y.L. Casallas-Moreno, M. de la L.O. Amador, Cu-Doped ZnO thin films deposited by a sol-gel process using two copper precursors: Gas-sensing performance in a propane atmosphere, Materials (Basel). 9 (2016). doi:10.3390/ma9020087.

[35] M. Babikier, D. Wang, J. Wang, Q. Li, J. Sun, Y. Yan, Q. Yu, S. Jiao, Cu-doped ZnO nanorod arrays: The effects of copper precursor and concentration, Nanoscale Res. Lett. 9 (2014) 1–9. doi:10.1186/1556-276X-9-199.

[36] M. Skompska, K. Zarębska, Electrodeposition of ZnO nanorod arrays on transparent

conducting substrates-a review, Electrochim. Acta. 127 (2014) 467–488. doi:10.1016/j.electacta.2014.02.049.

[37] A. Henni, A. Merrouche, L. Telli, S. Walter, A. Azizi, N. Fenineche, Effect of H2O2 concentration on electrochemical growth and properties of vertically oriented ZnO nanorods electrodeposited from chloride solutions, Mater. Sci. Semicond. Process. 40 (2015) 585–590. doi:10.1016/j.mssp.2015.07.046.

[38] A. Henni, A. Merrouche, L. Telli, A. Azizi, R. Nechache, Effect of potential on the early stages of nucleation and properties of the electrochemically synthesized ZnO nanorods, Mater. Sci. Semicond. Process. 31 (2015) 380–385. doi:10.1016/j.mssp.2014.12.011.

[39] A. Henni, A. Merrouche, L. Telli, A. Karar, F.I. Ezema, H. Haffar, Optical, structural, and photoelectrochemical properties of nanostructured ln-doped ZnO via electrodepositing method, J. Solid State Electrochem. 20 (2016) 2135–2142. doi:10.1007/s10008-016-3190-y.

[40] F. Ghahramanifard, O. Fazlolahzadeh, A. Rouhollahi, Electrodeposition of Cu-doped p-type ZnO nanorods; effect of Cu doping on structural, optical and photoelectrocatalytic property of ZnO nanostructure, Superlattices Microstruct. (2017). doi:10.1016/j.spmi.2017.07.019.

[41] M.F. Manzoor, E. Ahmad, M. Ullah, A.M. Rana, A.S. Malik, M. Farooq, I. Ahmad, M. Hasnain, Z.A. Shah, W.Q. Khan, U. Mehtab, Impact of copper doping on the structural, electrical and optical properties of auto-combustion synthesized ZnO nanocomposites, Acta Phys. Pol. A. 135 (2019) 458–466. doi:10.12693/APhysPolA.135.458.

[42] P. Jongnavakit, P. Amornpitoksuk, S. Suwanboon, N. Ndiege, Preparation and photocatalytic activity of Cu-doped ZnO thin films prepared by the sol-gel method, Appl. Surf. Sci. 258 (2012) 8192–8198. doi:10.1016/j.apsusc.2012.05.021.

[43] G.J. Chen, S.R. Jian, J.Y. Juang, Surface analysis and optical properties of Cu-doped ZnO thin films deposited by radio frequency magnetron sputtering, Coatings. 8 (2018). doi:10.3390/coatings8080266.

[44] G. Sigircik, O. Erken, T. Tuken, C. Gumus, O.M. Ozkendir, Y. Ufuktepe, Electrosynthesis of ZnO nanorods and nanotowers: Morphology and X-ray Absorption

Near Edge Spectroscopy studies, Appl. Surf. Sci. 340 (2015) 1–8. doi:10.1016/j.apsusc.2015.02.166.

[45] F.J. Humphreys, M.G. Ardakani, Grain boundary migration and zener pinning in particle-containing copper crystals, Acta Mater. 44 (1996) 2717–2727. doi:10.1016/1359-6454(95)00421-1.

[46] M. Chen, Z.L. Pei, C. Sun, L.S. Wen, X. Wang, Surface characterization of transparent conductive oxide Al-doped ZnO films, J. Cryst. Growth. (2000). doi:10.1016/S0022-0248(00)00834-4.

[47] A. Sreedhar, J.H. Kwon, J. Yi, J.S. Kim, J.S. Gwag, Enhanced photoluminescence properties of Cu-doped ZnO thin films deposited by simultaneous RF and DC magnetron sputtering, Mater. Sci. Semicond. Process. 49 (2016) 8–14. doi:10.1016/j.mssp.2016.03.023.

[48] N. Srinivasan, M. Revathi, P. Pachamuthu, Surface and optical properties of undoped and Cu doped ZnO nanostructures, Optik (Stuttg). 130 (2017) 422–426. doi:10.1016/j.ijleo.2016.10.080.

[49] Q. Ma, X. Yang, X. Lv, H. Jia, Y. Wang, Cu doped ZnO hierarchical nanostructures : morphological evolution and photocatalytic property, J. Mater. Sci. Mater. Electron. 0 (2018) 0. doi:10.1007/s10854-018-0503-1.

[50] M. Asgharian, M. Mehdipourghazi, B. Khoshandam, N. Keramati, Photocatalytic degradation of methylene blue with synthesized rGO/ZnO/Cu, Chem. Phys. Lett. (2019) 1–7. doi:10.1016/j.cplett.2019.01.037.

[51] S. Kumaresan, K. Vallalperuman, S. Sathishkumar, M. Karthik, P. SivaKarthik, Synthesis and systematic investigations of Al and Cu-doped ZnO nanoparticles and its structural, optical and photo-catalytic properties, J. Mater. Sci. Mater. Electron. 28 (2017) 9199–9205. doi:10.1007/s10854-017-6654-7.

[52] R.S. Ganesh, E. Durgadevi, M. Navaneethan, V.L. Patil, S. Ponnusamy, C. Muthamizhchelvan, S. Kawasaki, P.S. Patil, Y. Hayakawa, Tuning the selectivity of NH3 gas sensing response using Cu-doped ZnO nanostructures, Sensors Actuators, A Phys. 269 (2018) 331–341. doi:10.1016/j.sna.2017.11.042.

[53] P.R. Chikate, K.D. Daware, S.S. Patil, P.N. Didwal, G.S. Lole, R.J. Choudhary, S.W. Gosavi, R.S. Devan, Effects of Au loading on the enhancement of photoelectrochemical activities of the Au@ZnO nano-heteroarchitecture, New J. Chem. 44 (2020) 5535–5544. doi:10.1039/d0nj00004c.

[54] S. Zhuang, M. Lu, N. Zhou, L. Zhou, D. Lin, Z. Peng, Q. Wu, Cu modified ZnO nanoflowers as photoanode material for highly efficient dye sensitized solar cells, Electrochim. Acta. 294 (2019) 28–37. doi:10.1016/j.electacta.2018.10.045.

[55] A.N. Kadam, T.G. Kim, D.S. Shin, K.M. Garadkar, J. Park, Morphological evolution of Cu doped ZnO for enhancement of photocatalytic activity, J. Alloys Compd. 710 (2017) 102–113. doi:10.1016/j.jallcom.2017.03.150.